



HAL
open science

Self-Supported Electrocatalysts Derived from Nickel-Cobalt Modified Polyaniline Polymer for H₂-Evolution and O₂-Evolution Reactions

Razik Djara, Nathalie Masquelez, Marie-Agnès Lacour, Abdelhafid Merzouki, Julien Cambedouzou, David Cornu, Sophie Tingry, Yaovi Holade

► **To cite this version:**

Razik Djara, Nathalie Masquelez, Marie-Agnès Lacour, Abdelhafid Merzouki, Julien Cambedouzou, et al.. Self-Supported Electrocatalysts Derived from Nickel-Cobalt Modified Polyaniline Polymer for H₂-Evolution and O₂-Evolution Reactions. *ChemCatChem*, 2020, 10.1002/cctc.202001235 . hal-03009685

HAL Id: hal-03009685

<https://hal.science/hal-03009685v1>

Submitted on 23 Nov 2020

HAL is a multi-disciplinary open access archive for the deposit and dissemination of scientific research documents, whether they are published or not. The documents may come from teaching and research institutions in France or abroad, or from public or private research centers.

L'archive ouverte pluridisciplinaire **HAL**, est destinée au dépôt et à la diffusion de documents scientifiques de niveau recherche, publiés ou non, émanant des établissements d'enseignement et de recherche français ou étrangers, des laboratoires publics ou privés.

Self-Supported Electrocatalysts Derived from Nickel-Cobalt Modified Polyaniline Polymer for H₂-Evolution and O₂-Evolution Reactions

Razik Djara,^[a,b] Nathalie Masquelez,^[b] Marie-Agnès Lacour,^[c] Abdelhafid Merzouki,^[a] Julien Cambedouzou,^[b] David Cornu,^{*[b]} Sophie Tingry,^{*[b]} and Yaovi Holade^{*[b]}

[a] R. Djara, Prof. A. Merzouki
Laboratoire de Physico-Chimie des Hauts Polymères (LPCHP)
Université Ferhat Abbas Sétif 1
El Bez, Sétif 19000, Algeria

[b] R. Djara, N. Masquelez, Dr. J. Cambedouzou, Prof. D. Cornu, Dr. S. Tingry, Dr. Y. Holade
Institut Européen des Membranes, IEM UMR 5635, Univ Montpellier, ENSCM, CNRS, Montpellier, France
300 Avenue du Professeur Emile Jeanbrau, 34090 Montpellier, Cedex 5, France
E-mail: david.cornu@enscm.fr (D.C.), sophie.tingry@umontpellier.fr (S.T.), yaovi.holade@enscm.fr (Y.H.)

[c] Dr. M.-A. Lacour
ChemLab, Montpellier, France
ENSCM
240 Avenue du Professeur Emile Jeanbrau, 34296 Montpellier, Cedex 5, France

Supporting information for this article is given via a link at the end of the document

Abstract. The water splitting aims to produce H₂ for fuel cells and a number of industrial processes such as the ammonia synthesis and the metals refining. There is actually a major limitation about the development of cost-effective and efficient electrocatalysts to lower the cell voltage that must be overcome to perform sequentially the overall reaction that is 2H₂O → 2H₂ + O₂. In the present study, we combined Ni and Co as the promising alternative catalytic metals to Pt-group metals as well as N and S as the doping elements to fabricate self-supported electrocatalysts for hydrogen evolution (HER) and oxygen evolution (OER) in alkaline media. To these ends, the polymerization of the aniline into polyaniline (PANI) in the presence of Ni(II) and Co(II) followed by calcination in air resulted in the formation of heterogeneous catalytic materials self-supported onto a matrix made of C, N, S, Ni and Co. Enhanced activity and durability were recorded for the hybrid and bimetallic PANI-NiCo composite.

Introduction

The electrochemical approach emerges as a sustainable route for the production of hydrogen, which is a high-energy density fuel for clean electricity production and an important feedstock for the synthesis of platform chemicals.^[1] Yet, finding electrocatalytic materials that combine high activity, long-term durability and low cost is a challenging task as it would require foregoing precious metals, i.e. those of the platinum group. So among the conducting polymers, polyaniline (PANI) has received the most important interest in heterogeneous electrocatalysis during the last years.^[2] This interest is due to the fact that PANI can either be used directly as a support/electron relay because of its electrical conductivity,^[2d,3] or as a source of nitrogen doping after a well-controlled calcination phase.^[2c,4] One of the logical solution to augment the electrocatalytic performance is to incorporate Ni and/or Co species. Song *et al.*^[5] showed that the electro-polymerization of aniline onto a nickel foam significantly decreases the overpotential towards hydrogen evolution reaction (HER) of 0.1 V at a metric current density of 10 mA cm⁻² in comparison to the bar nickel electrode. Feng *et*

al.^[3f] reported that the modification of the CoP by PANI leads to a PANI-CoP material with high electrochemically active surface area and superior electrocatalytic activity towards HER in an acid medium. It was argued that PANI captures H⁺ species from hydronium ions to form protonated amine groups that have higher positive charge density than those of hydronium ions from the solution, thus accelerating the kinetics of HER at the PANI-CoP surface.^[3f] One can be summed up that the chemistry behind these strategies requires the co-material (e.g. CoP, nickel foam) to be prepared in advance and cannot be elegantly be generalized to metallic cations such Ni²⁺ or Co²⁺. Indeed, those ionic species could be readily lost during the electrocatalysis and decrease the catalytic activity and durability. Also, the above conclusion cannot meaningfully be implemented in alkaline media since the adsorption of H₂O molecules instead of H⁺ and their splitting is necessary (2H₂O + 2e⁻ → H₂ + 2HO⁻, E° = 0 V vs reversible hydrogen electrode (RHE)). Other limitations are the coverage of some active sites of the catalytic material by the PANI when the latter is deposited after the formation of metallic particles as well as the obvious absence of the creation of a strong metal-support interaction.

The emerged scenario to tackle the above limitations is the one-pot chemical polymerization in the presence of metallic cations followed by a proper thermal treatment to yield electrocatalysts with high activity.^[2c,4b,4e] We recently reported that the use of the ammonium persulfate (APS, (NH₄)₂S₂O₈) as the oxidizing agent and the nickel nitrate resulted in the fabrication of Ni₃S₂ species after thermal treatment at 700-1000 °C; and demonstrated an outstanding efficiency towards HER and oxygen evolution reaction (OER) in alkaline media.^[4b] Furthermore, nickel cobaltite (NiCo₂O₄) was studied for a long time as a promising electrode for O₂ electrocatalysis.^[6] The most utilized synthesis approach is the hydrothermal process combined with heat treatment (300-500 °C), which can lead to spinel nickel cobaltite with high water splitting activity (i.e. HER and OER).^[7] The origin of the high performance of Ni_yCo_{3-y}X₄ (X = O or S, 0 < y < 2) results from to synergetic effect arising from the mixed transition metal cations,^[6a,8] which enable controlling the adsorption of the reactants and the removal of the products.

N and S are known to allow the manipulation of the catalytic performance,^[9] however, precisely how both elements could be incorporated into the same material to target high efficiencies remains a puzzle.

Herein, we report the combination of the chemical polymerization of the aniline ($C_6H_5-NH_2$, C and N source) by the ammonium persulfate ($(NH_4)_2S_2O_8$, N and S source) in the presence of Ni(II)-Co(II) salts and the thermal treatment to fabricate a self-supported heterogeneous PANI-NiCo material as a multifunctional and efficient electrocatalyst for both HER and OER in alkaline media. The performed comprehensive structural characterization showed that the transformation at 550 °C under air allow converting the polymerization reaction mixture into a nanostructured carbon-sulfur-nitrogen network, which supports various Ni-Co-X ($X = O, S$) phases among which the bipyramid nickel cobaltite. This heterogeneous PANI-NiCo material demonstrated outstanding electrocatalytic activity and stability towards HER and OER in a basic electrolyte.

Results and Discussion

In order to synthesize a nanostructured matrix made of C, N, S, Ni and Co species, we implemented the chemical polymerization of the aniline in the presence of metallic precursors followed by the thermal treatment. Figure 1a resumes the adapted strategy for the synthesis. While the present study focuses on $NiCl_2 \cdot 6H_2O$ and $CoCl_2 \cdot 6H_2O$ precursors, the nitrate salts were however used in control synthesis. The mixture of the polymerization reaction underwent a solvent removal in a rotary evaporator to efficiently trap metal cations in the solid that will dry out afterwards at 80 °C. We previously found that this rotovap step is important because a simple filtration over Buchner results in the loss of Ni(II) and low yield of the synthesis.^[4b] The second step was the thermal treatment to allow the assembling of Ni and Co elements into Ni-Co-X ($X = O, S$) particles that are self-supported on a matrix made of C, N, S, Ni and Co. We hypothesized that the use of air as the environment for the thermal treatment instead of an inert gas such as nitrogen or argon will allow reaching an optimal compromise between the formation of a certain number of bipyramid nickel cobaltite particles onto a carbon-nitrogen-sulfur-oxygen-nickel-cobalt network and the removal of excess carbon, chloride, and sulfur species. Indeed, not only this thermal transformation defines the bonds in carbon-heteroatom but also the type of Ni- or Co-heteroatom junction, which all above will regulate the electrocatalytic performance. Seminal reports of Rasiyah *et al.*^[6c,8] showed that the $NiCo_2O_4$ spinel phase can be obtained by a freeze drying of a solution of nickel and cobalt nitrate followed by the vacuum decomposition and thermally treatment in air at 400 °C. Recent reports utilized the calcination under different conditions, 375 °C in air,^[10] 350 °C in Ar ,^[7a] 350 °C in N_2 ,^[7b] 400 °C (no indication of the type of gas that was used),^[7c] 350 °C in air,^[7d] and at 300 °C in air.^[11] It should be emphasized that the implementation of those temperatures of 350-400 °C in the present study could probably failed because the polyaniline material has complex behavior in this temperature range.^[12]

In order to clarify the above points, we conducted thermogravimetric analysis (TGA) and differential scanning calorimetry (DSC) analysis to probe the effect of the addition of

the metal precursor and the nature of the gas that should be utilized during the thermal treatment. Figures 1b and S1-S3 show the obtained results. The minor processes occurring below 150 °C are attributed to the evaporation of the water molecules that are adsorbed and/or trapped between the hydroscopic chains of the PANI polymer^[12-13] and confirm that the materials were well dried. Then, the elimination of the residual doping agent and the decomposition of smaller fragments of PANI occur at 200-350 °C with an endothermic peak at 241 °C while the degradation of the main chains takes place above 350 °C.^[12b,c] As hypothesized above, the introduction of nickel and cobalt salts triggers a positive shift towards 282 °C and 386 °C for the first peak and second peak, respectively. When the gas is nitrogen, these two peaks are located at 285 and 387 °C, respectively. Those findings could indicate that those Ni(II) and Co(II) species have an effect on the phenomena occurring there. Since this range of temperature regulates the rearrangement of the different atoms leading the bonds (carbon-carbon, carbon-nitrogen, nickel-sulfur, cobalt-sulfur, nickel-oxygen, and cobalt-oxygen), it became obvious that a temperature below 400 °C is not suitable for obtaining $Ni_yCo_{3-y}X_4$ ($X = O, S$). We conducted several control experiments, which demonstrated that the calcination under air at 550 °C was the optimal temperature. Unless otherwise specified, the next discussion focuses of the deep study of the physicochemical, electrochemical and electrocatalytic characteristics of the as-synthesized PANI-Ni, PANI-Co, and PANI-NiCo after calcination under air at 550 °C.

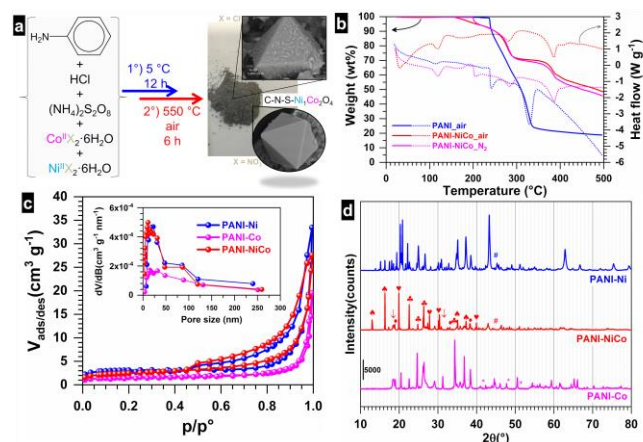


Figure 1. (a) Sketch of the used strategy for the synthesis of nickel cobaltite self-supported onto a matrix made of C, N, S, Ni and Co. (b) TGA (left y-axis, solid lines) and DSC (right y-axis, dotted lines) curves in an aluminum crucible in the range of 25-500 °C (5 °C min^{-1} , 100 mL min^{-1}). (c) N_2 adsorption-desorption isotherms and the corresponding pore size (diameter) distribution. (d) XRD patterns, see text for details.

We first utilized N_2 as probing molecule to access the textural properties of the as-synthesized PANI-Ni, PANI-Co, and PANI-NiCo materials. More specifically, we evaluated the specific surface area (the so-called Brunauer-Emmett-Teller, S_{BET} ($m^2\text{ g}^{-1}$)) as well as the pore volume and established the pore size distribution (Barrett, Joyner and Halenda (BJH)). Figure 1c shows the adsorption-desorption isotherms of N_2 on the different materials. The mesoporous character is evidenced by the slightly hysteresis loop. The extracted quantitative data are reported in Table S1. The determined surface area is $S_{BET} = 10$,

5, and 9 m² g⁻¹ for PANI-Ni, PANI-Co, and PANI-NiCo, respectively. The pore diameter (or pore size = 2×R_{B,H}) decreases as follows: PANI-Ni (47 nm) < PANI-Co (44 nm) < PANI-NiCo (29 nm). Those results suggest that the materials exhibit a mesoporous character. Furthermore, the pore volume is 0.049, 0.029, and 0.041 cm³ g⁻¹ for PANI-Ni, PANI-Co, and PANI-NiCo, respectively. It can be observed that the introduction of Co species in the PANI-Ni material enables decreasing the pore size from 44 to 29 nm while keeping the same pore volume and BET surface. The shape of the isotherms at lower pressures implies that the above volume mainly results from mesopores.

We then used powder X-ray diffraction (PXRD) to determine whether or not we succeeded in the preparation of a heterogeneous material comprising various structures including nickel cobaltite. Indeed, by using a relatively low calcination temperature of 550 °C, we were targeting the formation of Ni_yCo_{3-y}X₄ (X = O, S) to coexist with other species from C, N, S, O, Ni, and Co. Our goal was to release a material with multiple structures and capable of providing synergic effect during the catalysis. Figure 1d displays the PXRD patterns. Many peaks attributable to multiple crystalline structures with large lattice parameters appear in all patterns. Metallic fcc Ni (JCPDS 04-850) and hcp Ni (JCPDS 45-1027) are not clearly observable in the PXRD patterns of PANI-Ni and PANI-NiCo, as their main peak should show up at 44.8° (corresponding to (111) peak for the fcc phase and (011) peak for the hcp phase). Also, metallic fcc Co (JCPDS 15-0806) and hcp Co (JCPDS 05-727) are also not clearly visible in the PANI-Co and PANI-NiCo patterns. Therefore pure Co or Ni particles are not dominant, which was expected because the materials underwent calcination at 550 °C under air. The main crystal structures are rather composed of a complex mixture of sulfates, carbonates, hydroxides and carbohydroxides. A tentative indexation of the main peaks in the PANI-NiCo sample involves CoSO₄ (♣, JCPDS 46-0004), Ni₂CO₃(OH)₂·H₂O (otwayite, ♠, JCPDS 29-0868), Co₂CO₃(OH)₂ (♥, JCPDS 48-0083) and Ni(OH)₂ (♠, JCPDS 14-0117). Note that the main characteristic peaks (denoted by ↓ signs in Figure 1d) of the NiCo₂O₄ spinel structure (JCPDS 20-0781) could hardly be resolved in the PANI-NiCo sample. This would mean that the signal from the nickel cobaltite would be blurred into that of the other structures as explained above. Figure S4a shows the peaks at 18.9°, 30.9°, 36.7°, 38.3°, and 44.4°, correspond to the (111), (220), (311), (222), (400) planes, respectively, of NiCo₂O₄.

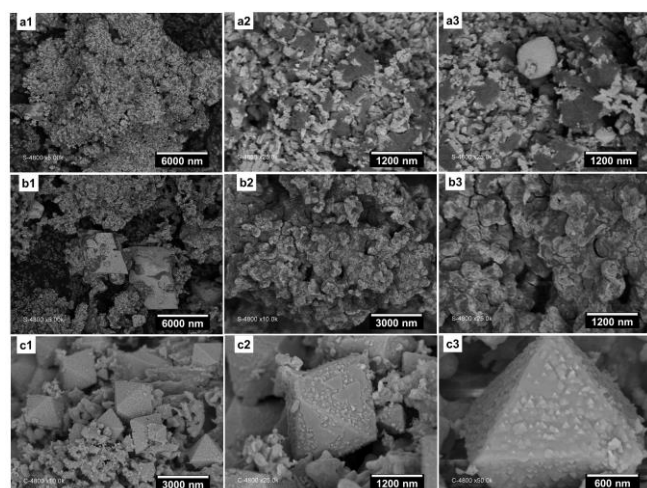


Figure 2. Backscattered SEM images of the as-synthesized materials. (a1-a3) PANI-Ni, (b1-b3) PANI-Co, (c1-c3) PANI-NiCo.

The gain a deep knowledge on the morphology of those PANI-based materials, the scanning electron microscopy (SEM) was used. Figure 2 shows the backscattered SEM images in order to make a better contrast between metallic and other species. The morphology of the material is in agreement with the data from the N₂ adsorption-desorption isotherms, especially the low BET surface of the PANI-Co. The first finding is that PANI-Ni and PANI-Co do not show any significant presence of bipyramid particles in comparison to PANI-NiCo. Additional backscattered SEM images reported in Figures S4a-S4d substantiate those observations. In other words, the simultaneous presence of Ni and Co is a prerequisite to obtain this structure. Similar shape was reported and attributed to NiCo₂O₄ octahedron exposing <111> crystal planes after complementary analysis by XRD, and high-resolution transmission microscopy.^[11] The control synthesis of PANI-NiCo materials performed at 350 °C (Figure S5, no obvious presence of bipyramid particles), 450 °C (Figure S6, no obvious presence of bipyramid particles), and 650 °C (Figure S7, presence of bipyramid particles), definitely underpins our postulated hypothesis that a temperature below 400 °C is not sufficient to generate the targeted particles. Finally, the backscattered SEM images of the control synthesis of PANI-NiCo material by the calcination at 550 °C under N₂ (Figure S8) reveal the presence truncated octahedron particles, which were previously reported to be NiCo₂O₄ exposing <111> and <100> crystal planes.^[11]

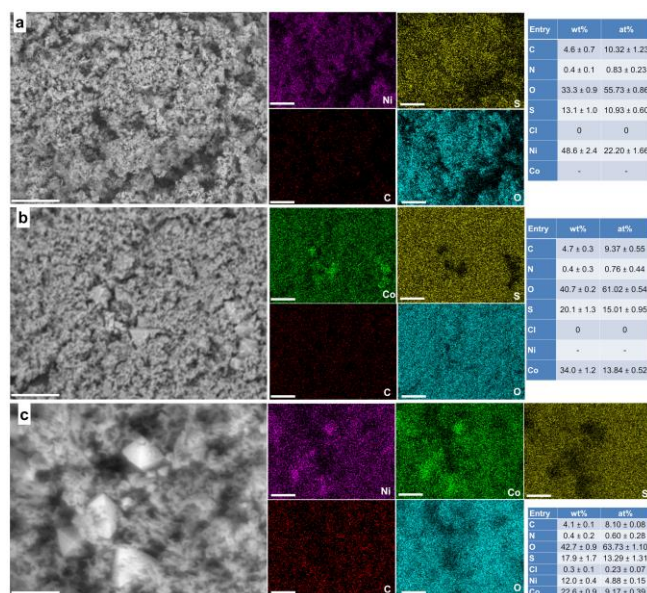


Figure 3. Backscattered SEM images; the corresponding micro-scale EDX mapping and quantitative composition of the materials: (a) PANI-Ni, (b) PANI-Co, and (c) PANI-NiCo. Scale bar = 10 μm.

The above SEM observations only provide a qualitative analysis of the materials. So, we next utilized the energy dispersive X-ray spectroscopy (EDX) to question whether a Ni_yCo_{3-y}O_{4-x}S_x heterogeneous could be obtained or not. Indeed, the simultaneous self-assembly of Ni and Co with O or S to form

$\text{Ni}_y\text{Co}_{3-y}\text{X}_4$ ($\text{X} = \text{O}, \text{S}$) is well-known to be more favorable than individual NiX_2 or CoX_2 .^[9a,11,14] As both S and O were present in the synthesis conditions, we specifically utilized the micro-scale EDX mapping to clarify the situation. Figures 3a-c depict the backscattered SEM images, the corresponding mapping and quantification of the Ni, S, C, O and Co for the three type of materials obtained under air at 550 °C, for instance, PANI-Ni, PANI-Co, and PANI-NiCo. By tracking the positions of S and Co, it can be clearly observed from Figures 3b and 3c that their mappings do not overlap. The result means that Co and S are not simultaneously present in the same structure. On the other hand, it can be seen in Figure 3c that the positions of the Co and Ni elements overlap perfectly with a significantly higher oxygen concentration than that of PANI-NiCo material obtained under N_2 . Those observations qualitatively rule out the formation of $\text{Ni}_y\text{Co}_{3-y}\text{O}_{4-x}\text{S}_x$ species, but support the obtaining of $\text{Ni}_y\text{Co}_{3-y}\text{O}_4$ that coexists with other nanostructured species.

The EDX spectra are reported in Figures S10-S14 and the main quantitative data are shown in Figure 3 (extended data are gathered in Table S2). The nitrogen content was $\text{N}(\text{at}\%) = 0.83 \pm 0.23, 0.76 \pm 0.44, \text{ and } 0.60 \pm 0.28$ for PANI-Ni, PANI-Co, and PANI-NiCo, respectively. The sulfur amount was found to be $\text{S}(\text{at}\%) = 10.93 \pm 0.60$ (PANI-Ni), 15.01 ± 0.95 (PANI-Co), and 13.29 ± 1.31 (PANI-NiCo). The found atomic ratio of $\text{Co}/\text{Ni} = 1.88 \pm 0.09, \text{ and } 2.37 \pm 0.12$ in PANI-NiCo obtained by thermal treatment under air and nitrogen confirm the theoretical expectation. It can however be observed that the $\text{O}/(\text{Ni}+\text{Co})$ atomic ratio of 2.52 ± 0.18 (PANI-Ni), 4.41 ± 0.13 (PANI-Co), and 4.54 ± 0.13 (PANI-NiCo) do not support the obtaining of a $\text{Ni}_y\text{Co}_{3-y}\text{O}_4$. For the monometallic PANI-Ni and PANI-Co materials, the EDX analysis suggests that metallic Ni and Co coexist with oxidized species. These outcomes are in agreement with the PXRD results that previously suggested the presence of multiple structures. The EDX profiles at the different places of the PANI-NiCo material and reported in Figure S13 confirm this hypothesis. Based on those physicochemical characterizations, it can be concluded that the thermal treatment of the polyaniline-based nickel-cobalt composites results in the formation of a heterogeneous materials. This heterogeneity is often very interesting from an electrocatalytic point of view when at least one reaction is targeted for the same material. This is the purpose of the present study where HER and ORR are targeted. In practice, this avoids having to change the electrode composition once the reaction is changed. So the next section aims to examine the electrochemical properties of those PANI-Ni, PANI-Co and PANI-NiCo materials.

The preceding discussion demonstrated that the optimal combination of the chemical polymerization and the thermal treatment allows synthesizing composite materials with different structures. Hence, we sought to study carefully the impact of this heterogeneity on the electrocatalytic ability towards two processes, HER and OER in alkaline media. Before investigating those electrocatalytic properties, we preliminary utilized the cyclic voltammetry (CV) as a powerful tool to determine their electrochemical characteristics. Figure S15 displays the recorded voltammograms at 50 mV s^{-1} scan rate in 1 M KOH electrolyte (25 °C). The electrode based on PANI-Co material does not show any significant redox peaks in comparison to the PANI-Ni, but there is a continuous increase of the current from 1 V vs RHE. For the PANI-Ni electrode, the pair of oxidation and reduction peaks between 1.2 and 1.5 V vs RHE

are historically attributed to the reversible electrochemistry of $\text{Ni}(\text{OH})_2$ hydroxide and NiOOH oxyhydroxide because the metallic nickel is irreversibly electrooxidized during the first cycle.^[15] For the bimetallic PANI-NiCo, the faradaic process associated to this oxyhydroxide/hydroxide significantly augments and the reduction peak shifts negatively of about 100 mV. This can be translated to as a synergic effect between nickel and cobalt species. Seminal studies of NiCo_2O_4 electrode attributed those redox processes to the simultaneous $\text{Co}^{2+}/\text{Co}^{3+}$ and $\text{Ni}^{2+}/\text{Ni}^{3+}$ transitions and even the $\text{Co}^{3+}/\text{Co}^{4+}$.^[8,16] It is known that the presence of two valence states on the sub-lattices and the possibility of excess oxygen in a NiCo_2O_4 spinel ($\text{Co}^{2+}_{1-x}\text{Co}^{3+}_x[\text{Ni}^{2+}_y \text{N}^{3+}_{1-y}\text{O}^{3+}_{1.0}]\text{O}^{2-}_4$ ($x=y$)) create a synergetic effect in this mixed transition metals, which enables regulating the adsorption of the reactants for a better electrocatalysis.^[6a,8,16] Based on the large electrical charge associated with the redox peaks of the PANI-NiCo material and thus a larger number of active sites, it is anticipated that this electrode will result in a better electrocatalytic performance. This especially applied to the case of OER whose electrocatalytic kinetics depends on what actually happens in the (oxyhydr)oxides region.

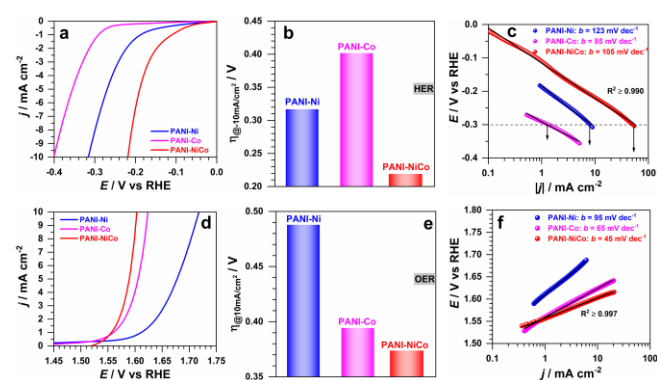


Figure 4. Catalytic ink deposited onto a carbon paper electrode. (a) HER polarization curves recorded at 5 mV s^{-1} . (b) Overpotential of HER at $j = -10 \text{ mA cm}^{-2}$: $\eta = E - E_{\text{eq}}$, $E_{\text{eq}} = 0 \text{ V vs RHE}$. (c) Tafel plots of HER. (d) OER polarization curves recorded at 5 mV s^{-1} . (e) Overpotential of OER at $j = 10 \text{ mA cm}^{-2}$: $\eta = E - E_{\text{eq}}$, $E_{\text{eq}} = 1.23 \text{ V vs RHE}$. (f) Tafel plots of OER. The electrolyte was 1 M KOH and the temperature was 25 °C.

To access the electrocatalytic activity towards HER and OER of the as-synthesized materials, the catalytic inks were firstly loaded onto a gas diffusion carbon electrode (carbon paper).^[17] Figures 4a-f shows the obtained results, which highlight the superior performance of the bimetallic PANI-NiCo as compared to the monometallic PANI-Ni and PANI-Co. The polarizations of HER in Figure 4a show that at $E = -0.3 \text{ V vs RHE}$, $j = -8.2, -1.4, \text{ and } -51.0 \text{ mA cm}^{-2}$ for PANI-Ni, PANI-Co, and PANI-NiCo, respectively. These data show that the achieved current with PANI-NiCo is 6.2 and 36.4 times higher in comparison to PANI-Ni and PANI-Co, respectively. Figure S16 reports the comparison with the state-of-the-art Pt/C catalyst. In Figures 4a,b and at the metric current density of $j = -10 \text{ mA cm}^{-2}$ that is employed in the literature to compared the efficiency in HER and OER,^[18] $E = -0.32, -0.40, -0.22, \text{ and } -0.09 \text{ V vs RHE}$ for PANI-Ni, PANI-Co, PANI-NiCo, and Pt/C, respectively. The determined Tafel slopes of 85-123 mV dec^{-1} (Figure 4c) suggest that the Volmer step is the rate determining step.^[18b] This can

explain the low overpotential of the bimetallic electrode where the presence of both metals at different valence states fosters the adsorption of H_2O molecules. For comparison, an overpotential of 250 mV at $j = -10 \text{ mA cm}^{-2}$ and a Tafel slope of 94 mV dec^{-1} were reported for NiCo_2O_4 octahedron.^[11] The summarized comparative performance of relevant HER on Ni-based catalysts from literature in alkaline solutions is reported in Table S3. The data indicate that the overpotential at $j = -10 \text{ mA cm}^{-2}$ ranges from 40 to 500 mV, which means that the present PANI-NiCo exhibits a promising efficiency. The polarization curves for OER in Figures 4d and S16b and the histograms of the overpotential at the metric current density of $j = 10 \text{ mA cm}^{-2}$ in Figure 4e show that $E = 1.72, 1.62, \text{ and } 1.60, 1.67 \text{ V vs RHE}$ for PANI-Ni, PANI-Co, PANI-NiCo, and Pt/C, respectively. Those results also point out the good performance of the PANI-NiCo material, which is also supported by the Tafel slope of 45 mV dec^{-1} ; Figure 4f. The comparison with relevant Ni-based catalysts from literature (Table S4, overpotentials of 215-400 mV and Tafel slopes of $36\text{-}87 \text{ mV dec}^{-1}$) shows that PANI-NiCo has an outstanding performance. Figure S17 reports the control analysis of the HER performance for PANI-NiCo materials obtained by thermal treatment under different atmospheres (air and nitrogen). The data highlight the superior activity of the material obtained by calcination in air, thus confirming the difference in the morphology as previously observed by SEM (Figure 2c1-c3 versus Figure S8a). Similar trend was reported for NiCo_2O_4 octahedron (enclosed by $\langle 111 \rangle$ faces) that has a higher activity than NiCo_2O_4 truncated octahedron (exposing $\langle 111 \rangle$ and $\langle 100 \rangle$ faces).^[11] Taken together, those set of results demonstrate that the as-synthesized heterogeneous bimetallic PANI-NiCo material can be used as a multifunctional electrocatalyst for both HER and OER.

The previous electrochemical measurements were based on a carbon paper substrate (gas diffusion electrode). This support works better for cathode reactions that do not required high electrode potentials, which could cause the oxidation of the carbon.^[17] To avoid/limit this deterioration of the support, the bulk nickel is widely used as supporting material, particularly for the water splitting reactions in alkaline electrolytes. So to fairly evaluate the durability of the PANI-NiCo that has shown the best performance in both HER and OER, the catalytic ink was loaded onto nickel foam (NF). Figures 5a-f show the obtained results. The used program for the accelerated durability test (ADT) consisted of a chronopotentiometry at $|j| = 10 \text{ mA cm}^{-2}$ for both HER (Figure 5b) and OER (Figure 5e). Figure 5a shows the recorded voltammograms of the fresh and aged electrodes. After the HER's ADT, the increase in the current density can be attributed to the reduction of the remaining oxidized surface species, the conditioning of the nickel-based electrode in a cathodic potential is routine in electrochemistry.^[15c] The presence of two anodic oxidation peaks after the OER's ADT can be attributed to the reorganization of the surface and is similar to the seminal observation at a NiCo_2O_4 -based electrode where the first anodic peak was assigned to a cobalt transition and the second oxidation peak was attributed to either cobalt or nickel transition given the different valence states.^[6a,8,16] Figure 5c shows that at $j = -10 \text{ mA cm}^{-2}$, $E = -0.26, -0.24, \text{ and } -0.18 \text{ V vs RHE}$ for NF_before-ADT, NF_after-ADT, NF-PANI-NiCo_before-ADT, and NF-PANI-NiCo_after-ADT, respectively. In other words, the overpotential decreases of about 60 mV after the HER's ADT for NF-PANI-NiCo, which is 3 times larger than

the blank NF (20 mV). This decrease can also be observed at $j = -50 \text{ mA cm}^{-2}$ and where $E = -0.4, -0.35, -0.32, \text{ and } -0.25 \text{ V vs RHE}$ for NF_before-ADT, NF_after-ADT, NF-PANI-NiCo_before-ADT, and NF-PANI-NiCo_after-ADT, respectively. At a much higher current density of $j = -100 \text{ mA cm}^{-2}$, $E = -0.42, \text{ and } -0.28 \text{ V vs RHE}$ for NF_after-ADT and NF-PANI-NiCo_after-ADT, respectively. Those results indicated that, after the electrode conditioning; a small overpotential of 280 mV is necessary to achieve a current density of 0.1 A cm^{-2} for a Tafel slope of 79 mV dec^{-1} (Figure 5d). For OER, the current density of $j = 10 \text{ mA cm}^{-2}$ was achieved at $E = 1.50, 1.66, 1.65, \text{ and } 1.62 \text{ V vs RHE}$ for NF_before-ADT, NF_after-ADT, NF-PANI-NiCo_before-ADT, and NF-PANI-NiCo_after-ADT, respectively (Figure 7f). The NF-PANI-NiCo maintains its Tafel slope of ca. 89 mV dec^{-1} after the ADT (Figure S18). Those results definitely confirm the excellent activity and stability of the as-synthesized heterogeneous PANI-NiCo as a multifunctional electrocatalyst for both HER and OER.

It was observed in this work that bipyramid NiCo_2O_4 particles contribute to a higher performance in comparison to the corresponding truncated octahedron particles. It is also well-known that nanostructured networks composed of carbon, nitrogen, and sulfur (in addition to nickel, and cobalt elements herein) provide good electrocatalytic performance towards both HER and OER. So, a unique structure-activity trend cannot be claimed for the as-prepared material PANI-NiCo given its heterogeneous nature.

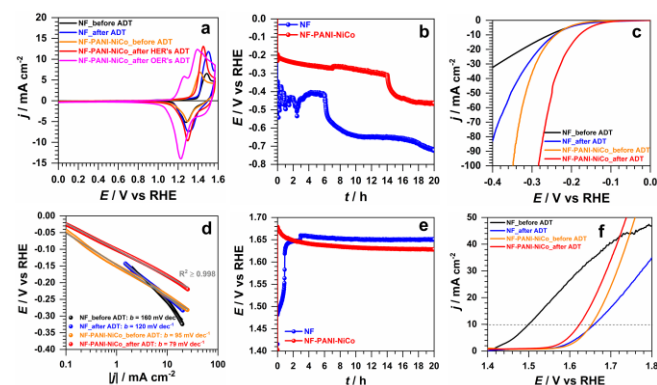


Figure 5. Catalytic ink deposited onto a nickel foam electrode. (a) iR-uncorrected CVs recorded at 50 mV s^{-1} . (b) Chronopotentiometry of HER at $j = -10 \text{ mA cm}^{-2}$ during the ADT. (c) HER polarization curves recorded at 5 mV s^{-1} . (d) Tafel plots of HER. (e) Chronopotentiometry of HER at $j = -10 \text{ mA cm}^{-2}$ during the ADT. (f) OER polarization curves recorded at 5 mV s^{-1} . The electrolyte was 1 M KOH and the temperature was $25 \text{ }^\circ\text{C}$.

Conclusion

We report a two-step sacrificial method to thermally convert the product of the polymerization of aniline in the presence of Ni(II) and Co(II) into an heterogeneous self-supported PANI-NiCo electrocatalyst for both HER and OER in alkaline media. The SEM observations showed that the conditions of the thermal treatment (temperature and gas) are the determining parameters for obtaining a bipyramid phase of nickel cobaltite NiCo_2O_4 self-supported onto a matrix made of C, N, S, Ni and Co. The optimized condition that makes a better comprise between the morphology of the particles and the electrocatalytic properties was the calcination at $550 \text{ }^\circ\text{C}$ under air. For HER, the potential

needed to achieved a metric current density of $j = 10 \text{ mA cm}^{-2}$ were found to be $E = -0.32, -0.40, -0.22,$ and -0.09 V vs RHE for PANI-Ni, PANI-Co, PANI-NiCo, and Pt/C (catalytic ink loaded onto a carbon paper substrate). For OER, the current density of $j = 10 \text{ mA cm}^{-2}$ was reached at $E = 1.72, 1.62,$ and $1.60, 1.67 \text{ V}$ vs RHE for PANI-Ni, PANI-Co, PANI-NiCo, and Pt/C. Those results clearly indicated that the performance of the bimetallic PANI-NiCo surpasses those of the monometallic PANI-Ni and PANI-Co, thus evidencing the synergic effect when nickel and cobalt are put together. Furthermore, the electrochemical measurements highlighted that after 20 h of accelerated durability test at $j = -10 \text{ mA cm}^{-2}$, the PANI-NiCo material (catalytic ink loaded onto a nickel foam) still exhibits high performance towards both HER and OER. Specifically, small overpotentials of 180 and 280 mV for current densities of 10 and 100 mA cm^{-2} were recorded for HER (Tafel slope of 79 mV dec^{-1}). This enhanced electrocatalytic characteristics of the PANI-NiCo material was attributed to its heterogeneous composition, which opens new directions towards the design of advanced self-supported electrocatalysts for the electrochemical hydrogen production.

Acknowledgements

This work at IEM Montpellier was supported by the CNRS Energy unit through the project PEPS19-ELECTROFUEL. D. Razik gratefully acknowledges the financial support from Campus France for his stay at IEM Montpellier through the program PROFAS B+ of "algéro-français cooperation". We thank Didier Cot (IEM Montpellier), Bertrand Rebiere (IEM Montpellier) Bernard Fraisse (Réseau des Rayons X et Gamma, Université de Montpellier) for assistance during SEM, EDX and XRD measurements.

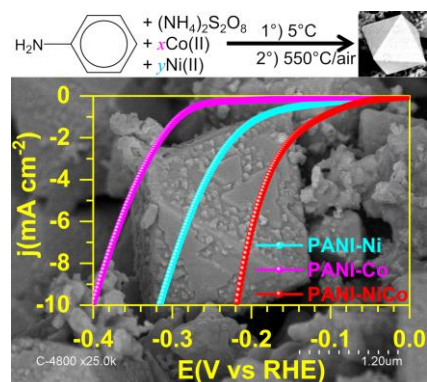
Conflict of Interest

The authors declare no conflict of interest.

Keywords: electrocatalysis • hydrogen evolution reaction • noble metal-free • oxygen evolution reaction • polyaniline

- [1] a) H. Wang, L. Gao, *Curr. Opin. Electrochim* **2018**, *7*, 7-14; b) J. Kwon, H. Han, S. Choi, K. Park, S. Jo, U. Paik, T. Song, *ChemCatChem* **2019**, *11*, 5898-5912; c) S. Dresp, F. Dionigi, M. Klingenhof, P. Strasser, *ACS Energy Lett.* **2019**, *4*, 933-942; d) C. Niether, S. Faure, A. Bordet, J. Deseure, M. Chatenet, J. Carrey, B. Chaudret, A. Rouet, *Nat. Energy* **2018**, *3*, 476-483; e) V. R. Stamenkovic, D. Strmcnik, P. P. Lopes, N. M. Markovic, *Nat. Mater.* **2017**, *16*, 57-69; f) Y. Holade, N. Tuleushova, S. Tingry, K. Servat, T. W. Napporn, H. Guesmi, D. Cornu, K. B. Kokoh, *Catal. Sci. Technol.* **2020**, *10*, 3071-3112.
- [2] a) K. S. Kim, Y. Hong, H. C. Kim, S.-I. Choi, J. W. Hong, *Chem. Eur. J.* **2019**, *25*, 7185-7190; b) M. Huang, H. Zhang, S. Yin, X. Zhang, J. Wang, *ACS Appl. Nano Mater.* **2020**, *3*, 3760-3766; c) J. Ma, M. Wang, G. Lei, G. Zhang, F. Zhang, W. Peng, X. Fan, Y. Li, *Small* **2018**, *14*, 1702895; d) X. Sun, N. Zhang, X. Huang, *ChemCatChem* **2016**, *8*, 3436-3440; e) D. Wang, L. Yang, H. Liu, D. Cao, *J. Catal.* **2019**, *375*, 249-256.
- [3] a) Q. Dang, Y. Sun, X. Wang, W. Zhu, Y. Chen, F. Liao, H. Huang, M. Shao, *Appl. Catal. B: Env.* **2019**, *257*, 117905; b) S. Chen, Z. Wei, X. Qi, L. Dong, Y.-G. Guo, L. Wan, Z. Shao, L. Li, *J. Am. Chem. Soc.* **2012**, *134*, 13252-13255; c) S. Xu, S. D. Minter, *ACS Catal.* **2014**, *4*, 2241-2248; d) Y. Liu, J. Li, F. Li, W. Li, H. Yang, X. Zhang, Y. Liu, J. Ma, *J. Mater. Chem. A* **2016**, *4*, 4472-4478; e) J.-X. Feng, L.-X. Ding, S.-H. Ye, X.-J. He, H. Xu, Y.-X. Tong, G.-R. Li, *Adv. Mater.* **2015**, *27*, 7051-7057; f) J.-X. Feng, S.-Y. Tong, Y.-X. Tong, G.-R. Li, *J. Am. Chem. Soc.* **2018**, *140*, 5118-5126.
- [4] a) R. Silva, D. Voiry, M. Chhowalla, T. Asefa, *J. Am. Chem. Soc.* **2013**, *135*, 7823-7826; b) R. Djara, Y. Holade, A. Merzouki, M.-A. Lacour, N. Masquelez, V. Flaud, D. Cot, B. Rebiere, A. van der Lee, J. Cambedouzou, P. Huguet, S. Tingry, D. Cornu, *Front. Chem.* **2020**, *8*, Article Number: 385; c) Z. Deng, Q. Yi, Y. Zhang, H. Nie, G. Li, L. Yu, X. Zhou, *Nano* **2018**, *13*, 1850006; d) J.-T. Ren, Z.-Y. Yuan, *ChemCatChem* **2018**, *10*, 3260-3268; e) J. Zhang, X. Meng, J. Zhao, Z. Zhu, *ChemCatChem* **2014**, *6*, 2059-2064; f) G. Wu, N. H. Mack, W. Gao, S. Ma, R. Zhong, J. Han, J. K. Baldwin, P. Zelenay, *ACS Nano* **2012**, *6*, 9764-9776.
- [5] F. Song, W. Li, G. Han, Y. Sun, *ACS Appl. Energy Mater.* **2018**, *1*, 3-8.
- [6] a) J. Haenen, W. Visscher, E. Barendrecht, *J. Electroanal. Chem. Interf. Electrochem.* **1986**, *208*, 323-341; b) J. G. D. Haenen, W. Visscher, E. Barendrecht, *J. Appl. Electrochem.* **1985**, *15*, 29-38; c) P. Rasiyah, *J. Electrochem. Soc.* **1983**, *130*, 2384.
- [7] a) J. Li, D. Chu, D. R. Baker, H. Dong, R. Jiang, D. T. Tran, *Chem. Mater.* **2019**, *31*, 7590-7600; b) J. Li, D. Chu, H. Dong, D. R. Baker, R. Jiang, *J. Am. Chem. Soc.* **2020**, *142*, 50-54; c) L. Tao, Y. Li, M. Li, G. Gao, X. Xiao, M. Wang, X. Jiang, X. Lv, Q. Li, S. Zhang, Z. Zhao, C. Zhao, Y. Shen, *J. Phys. Chem. C* **2017**, *121*, 25888-25897; d) X. Gao, H. Zhang, Q. Li, X. Yu, Z. Hong, X. Zhang, C. Liang, Z. Lin, *Angew. Chem. Int. Ed.* **2016**, *55*, 6290-6294.
- [8] P. Rasiyah, *J. Electrochem. Soc.* **1982**, *129*, 1724.
- [9] a) Y. Cui, Z. Liu, H. Guo, Y. Chai, C. Liu, S. Mintova, *ChemCatChem* **2019**, *11*, 5131-5138; b) J. Yao, L. Bai, X. Ma, M. Zhang, L. Li, G. Zhou, H. Gao, *ChemCatChem* **2020**, *12*, 609-614.
- [10] I. Abidat, C. Morais, C. Comminges, C. Canaff, J. Rousseau, N. Guignard, T. W. Napporn, A. Habrioux, K. B. Kokoh, *J. Mater. Chem. A* **2017**, *5*, 7173-7183.
- [11] L. Fang, Z. Jiang, H. Xu, L. Liu, Y. guan, X. Gu, Y. Wang, *J. Catal.* **2018**, *357*, 238-246.
- [12] a) R. Djara, Y. Holade, A. Merzouki, N. Masquelez, D. Cot, B. Rebiere, E. Petit, P. Huguet, C. Canaff, S. Morisset, T. W. Napporn, D. Cornu, S. Tingry, *J. Electrochem. Soc.* **2020**, *167*, Article number: 066503; b) X. Wang, D. Liu, J. Deng, X. Duan, J. Guo, P. Liu, *RSC Adv.* **2015**, *5*, 78545-78552; c) A.-u.-H. A. Shah, M. Kamran, S. Bilal, R. Ullah, *Materials* **2019**, *12*, 1527.
- [13] a) B. Lubentsov, O. Timofeeva, *Synth. Met.* **1991**, *45*, 235-240; b) E. C. Gomes, M. A. S. Oliveira, *Am. J. Polym. Sci.* **2012**, *2*, 5-13.
- [14] M.-Q. Wang, C. Ye, S.-J. Bao, Z.-Y. Chen, H. Liu, M.-W. Xu, *ChemCatChem* **2017**, *9*, 4169-4174.
- [15] a) M. Alsabet, M. Grden, G. Jerkiewicz, *Electrocatalysis* **2011**, *2*, 317-330; b) M. A. Abdel Rahim, R. M. Abdel Hameed, M. W. Khalil, *J. Power Sources* **2004**, *135*, 42-51; c) M. S. E. Houache, E. Cossar, S. Ntais, E. A. Baranova, *J. Power Sources* **2018**, *375*, 310-319.
- [16] J. Haenen, W. Visscher, E. Barendrecht, *J. Electroanal. Chem. Interf. Electrochem.* **1986**, *208*, 273-296.
- [17] D. Higgins, C. Hahn, C. Xiang, T. F. Jaramillo, A. Z. Weber, *ACS Energy Lett.* **2018**, *4*, 317-324.
- [18] a) X. Zou, Y. Zhang, *Chem. Soc. Rev.* **2015**, *44*, 5148-5180; b) Y. Shi, B. Zhang, *Chem. Soc. Rev.* **2016**, *45*, 1529-1541.

Entry for the Table of Contents



PANiNi & Co. Chemical polymerization of aniline into polyaniline in the presence of nickel-cobalt salts and calcination are combined to engineer self-supported electrocatalysts. The simultaneous presence of aniline and ammonium persulfate permits us to thermally convert, by a two-step sacrificial method, the reaction mixture into heterogeneous materials. The as-constructed framework composed of nickel cobaltite and a network of carbon, nitrogen, sulfur, nickel, and cobalt allows reaching high electrocatalytic performance towards water splitting reactions of H₂-evolution and O₂-evolution in alkaline media.